











Corrosion of diffusion zinc coatings in neutral chloride solutions

A.I. Biryukov,¹ * D.A. Zakharyevich,¹  R.G. Galin,² T.V. Batmanova,¹ 
V.E. Zhivulin,³  M.N. Ulyanov,¹  A.G. Fazlitdinova,¹  E.V. Zhizhin,⁴ 
A.V. Koroleva,⁴  I.A. Kasatkin⁴  and O.A. Kozaderov⁵ 

¹Chelyabinsk State University Br. Kashirins 129, 454001, Chelyabinsk, Russian Federation

²Vika Gal Ltd., ul. Molodogvardeytsev, 7454138, Chelyabinsk, Russian Federation

³South-Ural State University, Lenina Avenue 76, 454080, Chelyabinsk, Russian Federation

⁴St. Petersburg University, 7-9 Universitetskaya Embankment, 199034, Saint Petersburg, Russian Federation

⁵Voronezh State University, Universitetskaya square 1, 394018, Voronezh, Russian Federation

*E-mail: BiryukovAI.csu@yandex.ru

Abstract

The corrosion behavior of the diffusion zinc coatings based on the δ -phase FeZn_{7–10} in a solution of 3 wt.% NaCl in water was studied using electrochemical and physicochemical methods. Initial corrosion of the coatings involves selective dissolution of zinc from the δ -phase. As exposure duration increases, both components of the coating alloy dissolve. The physicochemical nature and electrochemical properties of the corrosion product layer were studied under conditions of simultaneous dissolution of the coating components. Iron can accumulate in the layer of corrosion products during prolonged corrosion of the coatings. In this case, the chemical composition of the electrolyte near the electrode and the structural and phase state of the corrosion products change. After long-term corrosion, the layer of products consisted of zinc oxide and amorphous hydroxide compounds of zinc and iron.

Received: January 12, 2024. Published: February 12, 2024

doi: [10.17675/2305-6894-2024-13-1-17](https://doi.org/10.17675/2305-6894-2024-13-1-17)

Keywords: corrosion, diffusion zinc coatings, corrosion products, sherardization

1. Introduction

Zinc coatings are used for anti-corrosion protection of steel products in construction, automotive, oilfield and other industries. Galvanic deposition, hot-dip galvanizing using zinc-filled polymer compositions, as well as thermal diffusion galvanizing produce zinc coatings. The last method known as sherardization has different advantages including no waste, environmental friendliness, uniform galvanizing of relief products, and produces Zn,Fe-coatings, which are so-called diffusion zinc (DZ) coatings based on the intermetallic δ -phase (FeZn_{7–10}) [1–6].

The corrosion resistance of zinc coatings in neutral environments is often associated with the protective properties of the layer of zinc corrosion products. A homogeneous, dense

layer of corrosion products with low electrical conductivity creates a barrier to aggressive particles, while the corrosion resistance of coatings increases. Traditionally the increase in corrosion resistance is associated with the barrier properties of layered zinc hydroxosalts. The chemical composition of salts depends on the chemical composition of the corrosive environment. For example, in a corrosive environment with a high concentration of Cl^- , basic zinc chloride (simonkolleite) is formed [7, 8], and in a corrosive environment with a relatively high concentration of CO_2 , basic zinc carbonate (hydrozincite) is formed [9–12]. The mechanism of formation of these corrosion products has been well studied for zinc and for zinc coatings with low concentrations of alloying components. The surface layers of hot zinc coatings consist of the η -phase, in which the concentration of iron is very low (>95.0 wt.% Zn) [1]. Therefore, the corrosion mechanism of pure zinc is used when describing the corrosion mechanism of hot zinc coatings.

At the same time, corrosion of zinc alloy coatings with a high concentration of alloying component, such as, for example, DZ coatings can be accompanied by selective dissolution of zinc [13–16]. Its effect can be negative, leading to accelerated corrosion, or positive, increasing corrosion resistance due to the accumulation of a more electropositive component on the surface. The influence mechanism of alloying components of zinc coatings on their corrosion resistance is poorly understood in this case, and the approaches to describe this effect are rather controversial. According to some authors, the alloying component increases the density of the layer of corrosion products; on the other hand, the authors suggest that the alloying component reduces the electrical conductivity of the layer of corrosion products. The purpose of this work is to study the influence of the alloying component (iron) on the corrosion behavior of DZ coatings in neutral chloride-containing aqueous solutions. This work is a continuation of studies of the corrosion behavior of DZ coatings in slightly acidic [17] and alkaline solutions [18].

2. Material and Methods

As in our previous works [17, 18], we used the author's sherardization technology to obtain DZ coatings [19]. Only Zn powder with a hydrothermally treated particle surface [19, 20] was used for coating. A layer of zinc oxide forms on particles of zinc powder during hydrothermal treatment. The zinc oxide layer prevents zinc particles from sticking together when heated and increases the zinc vapor pressure. This allows one to avoid the use of activators and fillers. The technology and process of coating are described in detail in [17–20]. The technology makes it possible to obtain uniform, homogeneous coatings with high adhesion based on the δ -phase with a thickness of up to 100 microns. Such coatings not only have high protective properties, but also are convenient objects for studying the corrosion of iron-zinc alloys and the influence of films of corrosion products on the process.

2.1. Coatings samples preparation

Steel St20 was used as a substrate for DZ coatings. Samples were made in the form of disks with a diameter of 20.0 mm and a thickness of 3.0 mm with a hole for hanging. Their surface

was sanded and degreased with isopropyl alcohol. The geometric parameters of the samples were measured with an accuracy of 0.01 cm and the surface area was calculated. The weight of the samples was determined before and after coating treatment with an accuracy of 0.1 mg. The thickness of the coating was calculated from the difference in mass before and after coating. We used hydrothermally treated zinc powder of the PZR-1 brand; the particle size ranged from 10 to 40 μm , and the thickness of zinc oxide films on metal particles was $\sim 1 \mu\text{m}$ [19, 20]. Steel samples and zinc powder were loaded into a laboratory furnace and heated to 420°C. After processing, the samples were cooled in an oven. Before all tests, coated samples were sanded with P1200 and P2500 sandpaper and degreased with isopropyl alcohol.

2.2. Characterization of the coatings

The atomic fractions of iron and zinc in the surface intermetallic layer of the samples were determined by X-ray fluorescence spectrometry using an ARL QUANT'X Energy-Dispersive XRF Spectrometer (Thermo Scientific) at accelerating voltage of 20 kV. The surface of the coatings before and after the corrosion tests was studied using a JEOL JSM7001F scanning electron microscope equipped with an Oxford INCA X-max 80 energy dispersive X-ray fluorescence spectrometer for elemental analysis. X-ray diffraction analysis of the DZ coatings and of their corrosion products was performed with a Bruker D8 Discover diffractometer with Cu $K\alpha$ -radiation, within the 2θ range of 10° – 125° .

2.3. Corrosion tests

- 1) Coatings with thickness of 40–45 μm were weighed with an accuracy of 0.0001 g, their geometrical parameters were measured with an accuracy of 0.01 cm. The coatings with surface area of $10 \pm 0.5 \text{ cm}^2$ were exposed in 0.5 dm^3 polypropylene containers with a solution of 3 wt.% sodium chloride in water at $20 \pm 2^\circ\text{C}$ under air. The electrolyte was not changed during the whole period of exposure, and the samples remained completely immersed in it for 1, 2, 3, and 6 months.
- 2) After removal from the solution, the coatings were washed with distilled water and air-dried. The samples were divided into two parts. The first part of samples was used for studying the electrochemical and corrosion behavior of the coatings (the methods are described in Section 2.4). The second part was used for physical and chemical characterization of the corrosion products (the methods used for studying morphology, chemical and phase composition are described in Section 2.5).
- 3) The corrosion products were further removed mechanically and by washing in a hydroxylamine solution. The corrosion rate ($\text{g}/\text{m}^2 \cdot \text{hour}$) was determined gravimetrically from a decrease in the sample weight.

2.4. Electrochemical measurements

The open circuit potential and polarization curves were measured after the exposition of the coatings in 3 wt.% NaCl solution without removing the film of corrosion products. Then the corrosion products were removed and the same measurements were repeated. The resistance of the corrosion product layer was determined by electrochemical impedance spectroscopy.

2.4.1. Open circuit potential (OCP) and polarization curves

Potentiostat-galvanostat Elins P-30J and clamp cell was used for the electrochemical tests. OCP was measured for 1 h, and the polarization curves were measured from the cathodic (-1.5 V vs. SHE) to the anodic region (-0.3 V vs. SHE) at a scan rate of 0.005 V \cdot s $^{-1}$. The experiments were carried out at a temperature of $20 \pm 2^\circ\text{C}$ under air. The potential was measured with respect to a silver/silver chloride reference electrode with a saturated KCl solution. The potentials are given relative to a standard hydrogen electrode. The counter electrode was graphite. The curves were plotted in the semi-logarithmic coordinates E – $\lg i$, and the corrosion current (i_{corr} , mA/cm 2) was determined from the intersection of the Tafel sections of the anodic and cathodic curves.

2.4.2. Impedance spectroscopy

The impedance spectra were obtained using an Elins Z-1500J impedance meter in a clamp cell with a graphite counter electrode in the frequency range from 10 mHz to 20 kHz with an alternating signal amplitude of 20–100 mV.

2.5. Characterization of the corrosion products

Scanning electron microscopy (Section 2.2), X-ray diffraction (Section 2.2), FTIR-spectroscopy and Photoelectron spectroscopy were used for characterization.

2.5.1. FTIR-spectroscopy

Corrosion products were removed from the sample surface, pressed with KBr (dried at 200°C for 5 hours), and studied using a Shimadzu IRAffinity-1S infrared spectrophotometer within the measurement range from 400 cm $^{-1}$ to 4000 cm $^{-1}$. The device resolution was 4 cm $^{-1}$, the number of scans was 100.

2.5.2. Photoelectron spectroscopy

The XPS measurements of the coating corrosion products were conducted at the Resource Center “Physical Methods of Surface Investigation”, St. Petersburg State University, using the photoelectron spectrometer “Escalab 250Xi” with a monochromatic AlK α radiation (photon energy is 1486.6 eV). The spectrometer was calibrated on the Au 4f $_{7/2}$ standard line (binding energy is 84.0 eV). The spectra were recorded in the constant pass energy mode at 50 eV, using XPS spot size of 650 μm . A total energy resolution of the experiment was about 0.3 eV. Measurements were performed at room temperature in an ultrahigh vacuum of the order of $1 \cdot 10^{-9}$ mbar. The combined ion-electronic charge compensation system was used to remove the sample charge.

3. Results

3.1. Characterization of the coatings

The concentration of zinc in the surface layers of coatings, according to X-ray fluorescence spectroscopy, was 89.0 ± 2.2 at.% with a DZ coating thickness of 20 μm ; 92.30 ± 0.03 at.% with a thickness of 40–45 μm and 92.9 ± 0.2 at.% with a thickness of 80–90 μm . In the range of zinc concentrations of 88.5 and 93.0 at.%, there is a δ -phase, according to the phase diagram of the Fe–Zn system [1]. Thus, the chemical composition of the surface layers of DZ coatings with a thickness of 20 to 100 μm is in the concentration range of the δ phase. In Figure 1 shows X-ray diffraction patterns of DZ coatings of various thicknesses. It can be seen that the phase composition of the surface layers is indeed represented by the δ phase (ICDD No. 01-083-4808). In further studies, coatings with a thickness of 40–45 μm were used, because this is the thickness used in industry.

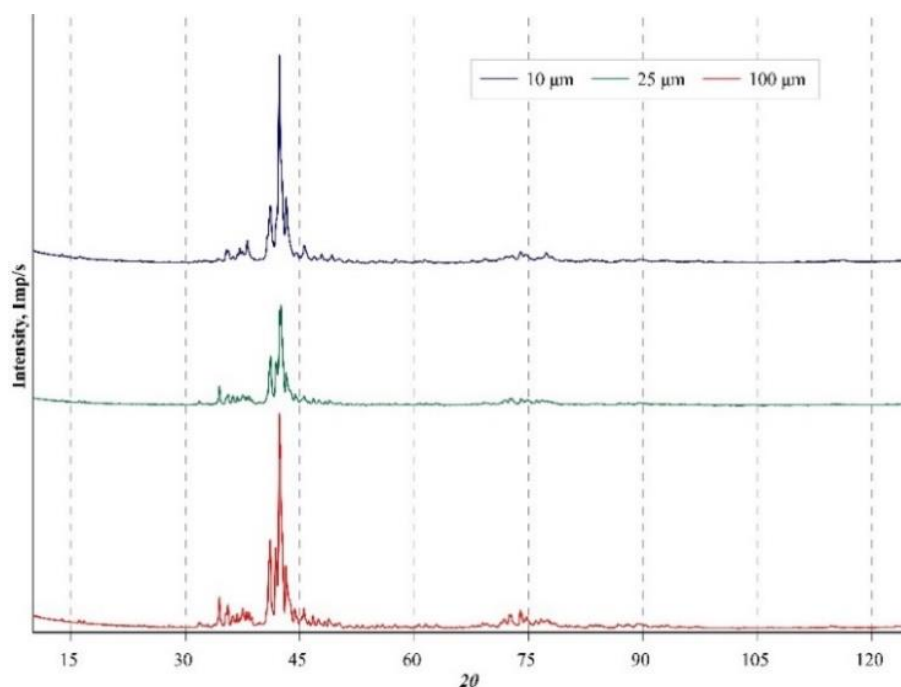


Figure 1. X-Ray diffraction patterns of DZ coatings with different thickness.

3.2. Corrosion and electrochemical behavior

Table 1 presents the corrosion rate V_{corr} ; open circuit potentials (OCP) E_{ocp} ; corrosion current densities i_{corr} ; components of equivalent electrical circuits of the coatings: R_s – electrolyte solution resistance; R_{tr} – resistance of ion transport through the corrosion products layer; R_{ct} – charge transfer resistance at the interface of the layer of corrosion products/solution.

The corrosion rate calculated from the loss of mass coating decreased over time, but the decrease rate was less than 15% over 6 months of exposure.

Table 1. Corrosion and electrochemical parameters of the DZ coating after exposition in 3 wt.% NaCl.

Parameter	Time, months			
	1	2	3	6
V_{corr} , g/m ² ·h	0.054	0.048	0.045	0.046
E_{ocp} with products corrosion layer, mV	–531	–456	–376	–388
E_{ocp} without products corrosion layer, mV	–575	–600	–540	–670
i_{corr} with products corrosion layer, mA/cm ²	0.35	0.32	0.31	0.25
i_{corr} without products corrosion layer, mA/cm ²	0.21	0.47	0.71	0.73
R_s , Ohm	21.5	28.8	26.1	20.1
R_{tr} with products corrosion layer, Ohm	2457	2900	1748	352.8
R_{ct} with products corrosion layer, Ohm	4188	1057	1838	856.6

The OCP of the DZ coating before exposure (–721 mV) was close to that of zinc in a solution of 3 wt.% NaCl (–800 mV [21]). As exposure increased, the potential became more positive. The change in potential occurred more intensely during the first 3 months of exposure. When the exposure time increased to 6 months, the potential changed by only 12 mV. The change in potential was associated with dezincification of the coating and the formation of a layer of corrosion products and removing them caused the potential to become more negative.

Figure 2 shows the polarization curves of DZ coatings in 3 wt.% NaCl solution before and after removal of the corrosion product layer. It can be seen that anodic polarization of the coating leads to an increase in the anodic current and to the appearance of an anodic peak at the potentials of –1050 to –1080 mV. The anodic peak corresponds, probably, to the oxidation of zinc. For the coatings with a corrosion product layer, the peak height decreased with time. Removing the layer led to a three times increase in the anodic peak intensity. A decrease in the anodic current by 1.5–2 times was observed in the potential interval of 300 mV, then the current increased. The intersection of the Tafel sections of the cathodic and anodic curves shows the corrosion current. It decreased by 1.4 times with increasing exposure for the coatings with a corrosion product layer. Removing the corrosion product layer led to an increase in the current at all exposures, except for the 1-month exposure.

Figure 3 shows the impedance spectra of DZ coatings for different exposure times. The spectra have the form of elongated semicircles with the centers below the x-axis. Figure 4 shows an equivalent electrical circuit of the corrosion process used for calculating the polarization resistance. The circuit consists of a resistance which is connected in series with a part of the circuit, consisting of a capacitance and resistance connected in parallel, which, in turn, is connected in series to the resistance of a layer of corrosion products. The first element shows the properties of the outer layer of corrosion products, which is in contact

with the electrolyte. They are caused by the resistance of ion transport and the electric double layer described in the circuit by the constant phase element (CPE). The second element corresponds to the layer of corrosion products that is adjacent to the coating surface. Thus, this scheme simulates a layer of corrosion products divided into two parts. CPE probably arises due to the distribution of the time constant, since all the recorded spectra are not purely capacitive in nature. Therefore, a constant phase element (CPE) was used instead of a capacitor to describe the electric double layer. The use of CPE is often required due to the inhomogeneity of the interface caused by surface roughness, hydration phenomena, complex structure and, as a consequence, uneven distribution of reaction rates and current on the corroding surface.

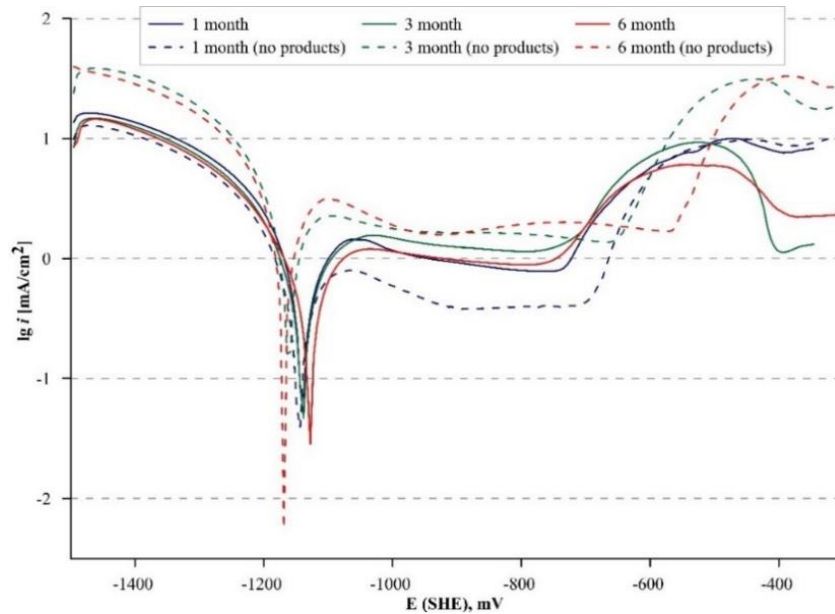


Figure 2. Polarization curves of the DZ coatings after different exposure time in 3 wt.% NaCl.

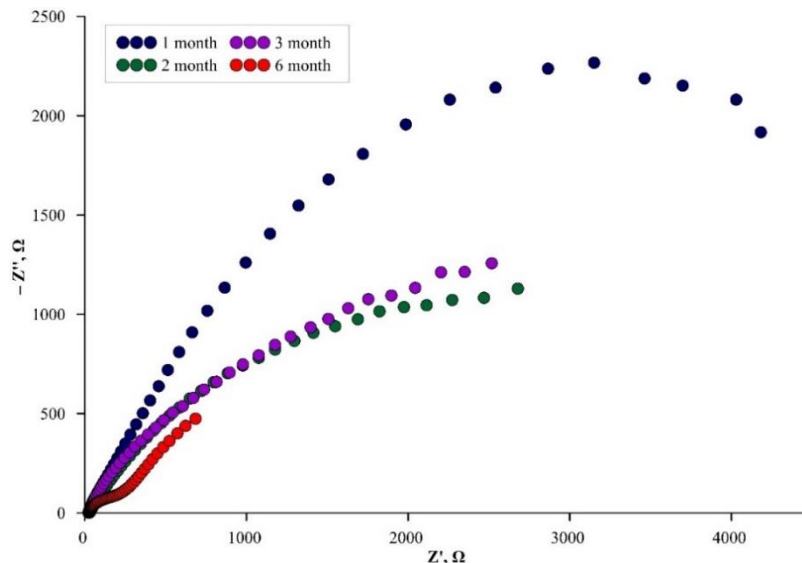


Figure 3. EIS spectra of the DZ coatings after different exposure time in 3 wt.% NaCl.

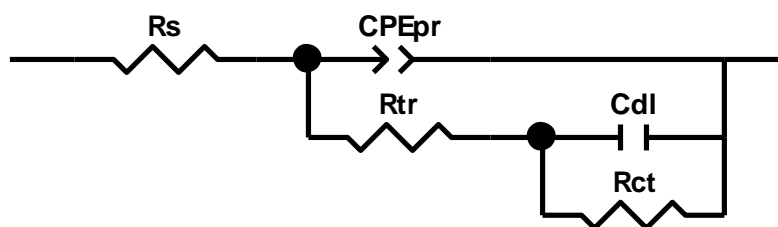


Figure 4. Equivalent electric circuit used to simulate the EIS data obtained for the DZ coatings. CPE_{pr} – constant phase element; R_s – resistance of the electrolyte solution; R_{tr} – resistance of ion transport through the corrosion products layer; R_{ct} – resistance to charge transfer at the interface of the layer of corrosion products/solution; C_{dl} – capacity of the double layer at the film/solution interface.

Table 1 shows the equivalent circuit parameters for different exposures. Resistance R_s has a maximum at 2 months of exposure and then decreases to 20 Ohms, which is close to the initial value. This may be due to the chemical binding of ions into insoluble precipitates. The resistance of ion transport through the corrosion products layer (R_{tr}) also has a maximum after exposure for 2 months. With an exposure of 6 months, the resistance R_{tr} decreases almost by 10 times. Resistance R_{ct} has a complex dependence on exposure time, but also decreases slightly with increasing exposure time to 6 months.

3.3. Analysis of the corrosion products

3.3.1. Scanning electron microscopy of the coatings after corrosion

Figure 5 shows SEM images of the surface of DZ coatings after exposure to a 3 wt.% NaCl for 1, 3 and 6 months and removal of corrosion products layer.

The coating surface becomes morphologically heterogeneous after 1 month of exposure (Figure 5a). This is typical of corrosion of alloys with selective dissolution of zinc. The roughness of the coating surface increases with increasing exposure to the corrosive environment. Corrosion pits increase in size and have clearer boundaries (Figure 5b) after 3 months of exposure. Pits can become centers of crystallization of corrosion products. Elongated crystals with the length of about 1 μm with hexagonal facets of 0.1 μm in size are present inside the pits (Figure 5d). Thus, selective dissolution of an alloy component can create centers of crystallization of the corrosion products. The surface morphology, as well as the unremoved corrosion products, can affect the shape of the polarization curves (Figure 2). Analysis of the coating surface after exposure for 3 months did not show large cracks or exposure of the steel substrate. The Zn:Fe concentration ratio determined by micro-X-ray analysis of the surface was 12.5:1, which was close to the initial Zn:Fe ratio in the δ phase. After exposure for 6 months, the surface of the DZ coating became loose and uneven. Areas of open steel substrate and cracks were observed on the surface. The Zn:Fe concentration ratio was 1:1, according to X-ray microanalysis.

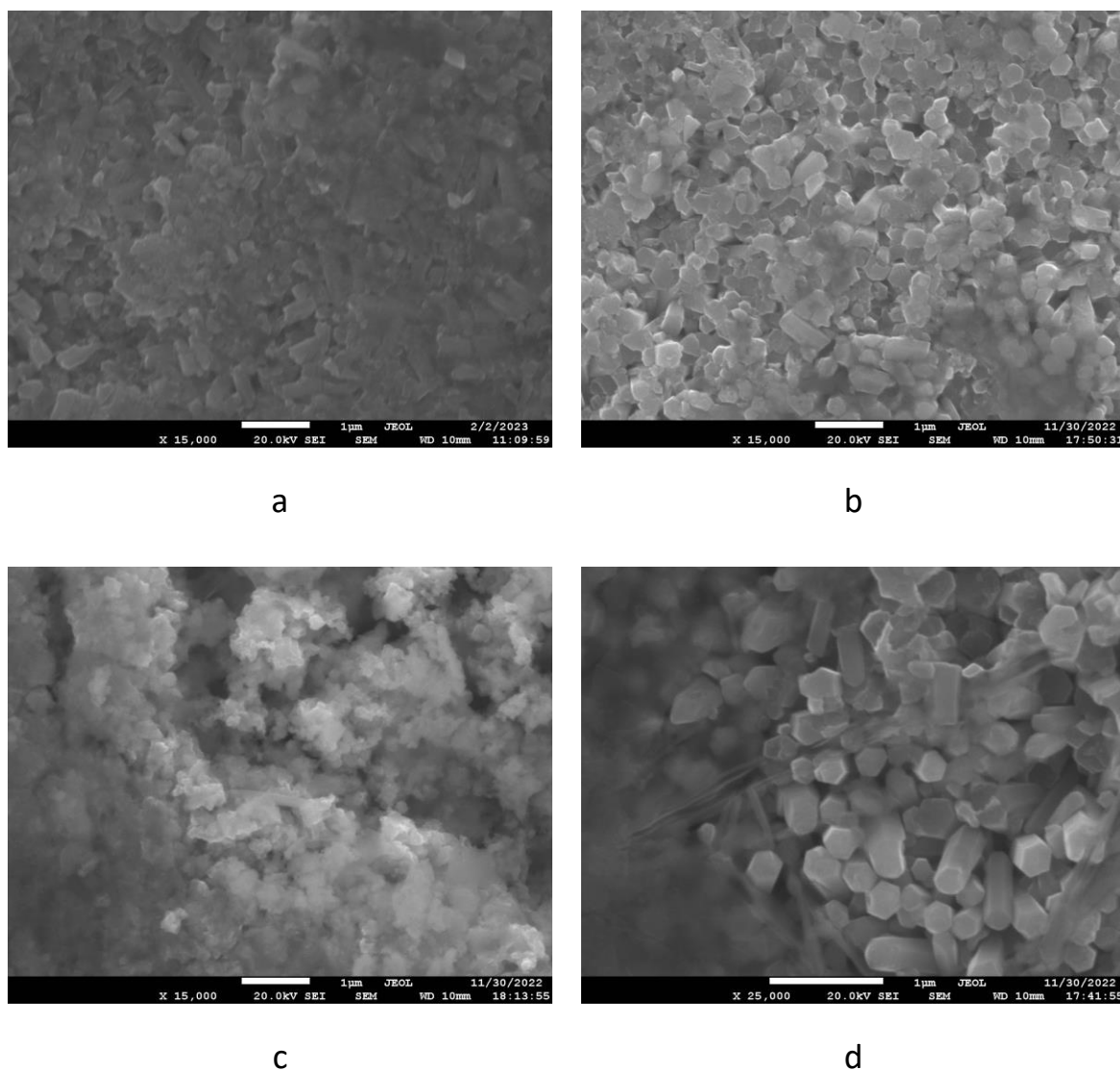


Figure 5. SEM images of the DZ coating after exposure in 3 wt. % NaCl of different duration: *a* – 1 month; *b*, *d* – 3 months; *c* – 6 months.

3.3.2. FTIR-spectroscopic characterization of the corrosion products

Figure 6 shows the IR spectra of corrosion products of DZ coatings after exposure to a 3 wt.% NaCl for 1, 2, 3 and 6 months (the spectrum number in the text corresponds to the exposure time).

The absorption band at the frequencies of $3600\text{--}3200\text{ cm}^{-1}$ corresponds to the stretching vibrations of OH^- [22, 23]. In spectrum 1, the band $3600\text{--}3200\text{ cm}^{-1}$ broadens, and the peak frequency is 3396 cm^{-1} , which is characteristic of $\text{Zn}(\text{OH})_2$ [24]. As exposure increases, the band becomes sharper, the peak frequency shifts by 100 cm^{-1} , and the intensity increases. The absorption band splits in spectrum 6. The shift of the absorption bands shows that the stretching vibrations of the OH group belong to $2\text{ZnOHCl}\cdot 3\text{Zn}(\text{OH})_2$ [24]. This compound is similar to simonkolleite ($\text{ZnCl}_2\cdot 4\text{Zn}(\text{OH})_2\cdot \text{H}_2\text{O}$). Band splitting may be due to

the simultaneous presence of $\text{Zn}(\text{OH})_2$ and ZnOHCl , which form $2\text{ZnOHCl} \cdot 3\text{Zn}(\text{OH})_2$. The cause of splitting may be intermolecular interaction in the unit cell of a substance. The authors of [25] showed that the splitting of this absorption band was associated with the formation of simonkolleite.

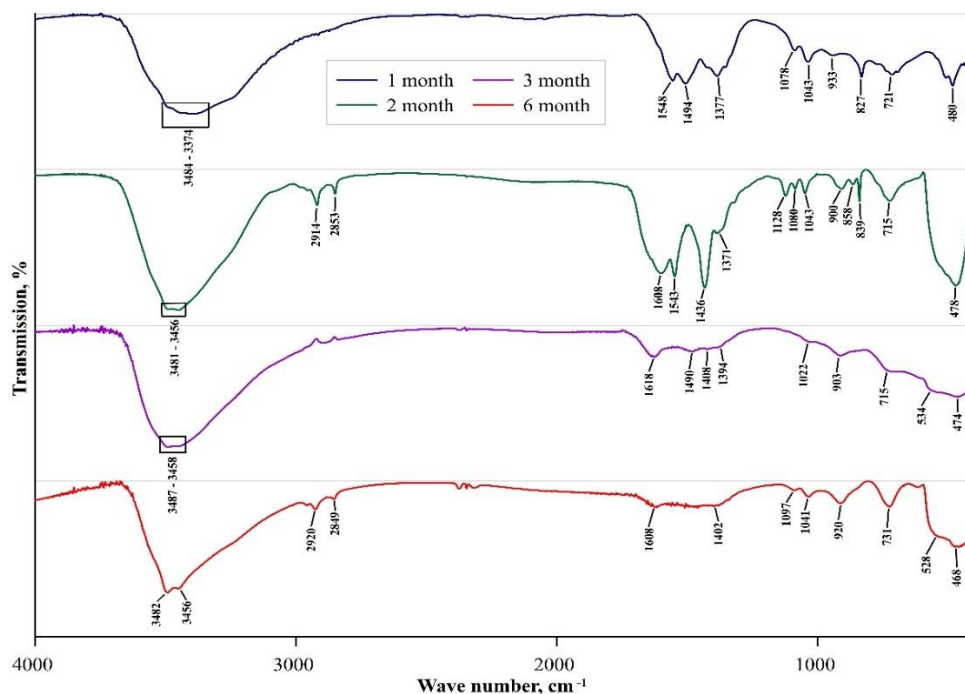


Figure 6. FTIR spectra of the corrosion products formed on the DZ coatings after exposure in 3 wt.% NaCl of different duration.

The absorption bands at the frequencies of $2925\text{--}2850\text{ cm}^{-1}$ have low intensity and are present only in spectra 2 and 6. They correspond to the stretching vibrations of the OH group in $\text{Zn}(\text{OH})_2$. A doublet may appear due to the heterogeneity of the corrosion products distribution or due to adverse chemical reactions.

The absorption band at the frequencies of $1625\text{--}1555\text{ cm}^{-1}$ corresponds to bending vibrations of OH^- . With increasing exposure, the absorption band shifts to higher frequencies. In comparison with the absorption band in the region of $1547\text{--}1382\text{ cm}^{-1}$, this band is poorly resolved. The authors of [22] attribute the absorption band at 1620 cm^{-1} to simonkolleite. The authors of [21] showed that this band corresponded to deformation vibrations of H_2O in the interlayer space of basic zinc salts. An increase in the intensity of this absorption band may indicate an increase in the number of water molecules.

The absorption band at the frequencies of $1547\text{--}1382\text{ cm}^{-1}$ corresponds to vibrations of the C–O bond in hydrozincite $\text{Zn}_5(\text{OH})_6(\text{CO}_3)_2$ [26–30]. The authors of [22, 23, 28, 31] showed that the absorption bands at the frequencies of 1380 cm^{-1} and 1510 cm^{-1} belonged to asymmetric stretching vibrations of the C–O bond in CO_3^{2-} . The highest intensity of the bands in this range was observed after 2 months of exposure. As the exposure time increased further, the intensity of the absorption band decreased until it disappeared completely.

The absorption bands at the frequencies of 1122–1088 cm^{-1} are present in spectra 1 and 2. The authors of [25] attributed the vibrations in the region of 1000–700 cm^{-1} to the Zn–O–H bond. The authors of [26, 28] attributed three characteristic absorption bands between 1100 and 600 cm^{-1} to simonkolleite. There are no absorption bands at these frequencies in spectra 3 and 6.

The absorption band at the frequencies of 1048–1033 cm^{-1} corresponds to bending vibrations of Zn–OH in simonkolleite. Absorption bands in the frequency range of 920–715 cm^{-1} correspond to deformation vibrations in simonkolleite, according to [23, 24, 27, 32]. At the same time, the absorption bands at 1040, 840 and 730 cm^{-1} were attributed to hydrozincite [27, 28, 31]. The authors showed [29] that hydrochloride contaminated with CO_3^{2-} had absorption bands at 1593, 1492, 1388, 1026 and 707–735 cm^{-1} . At the same time, hydrozincite has an absorption bands at 1558, 1489, 1375, 1303, 1031 and 831 cm^{-1} . The intensity of these absorption bands decreased with increasing exposure time.

The absorption band at the frequencies of 482–458 cm^{-1} is wide and has a high intensity. A clear resolution of this band can be observed after sample exposure for 1 month. Absorption bands in the region of 600–350 cm^{-1} relate to the Zn–O bond in ZnO oxide [25–29, 32, 33]. At the same time, a broad band may consist of narrow absorption bands of Zn–O and Zn–Cl bonds.

3.3.3. XRD characterization of the corrosion products

Figure 7 shows X-ray powder diffraction patterns of coating corrosion products after exposure to 3 wt.% NaCl for 1, 2, 3 and 6 months.

The ZnO peaks have the highest intensity in all X-ray diffraction patterns. In addition, all XRD patterns contain NaCl and ZnCl_2 peaks, but their intensity decreases with the exposure time. They disappeared from XRD after 6 months of exposure. The peak at $2\theta \sim 11.5^\circ$ is present in all X-ray diffraction patterns. Its position is close to the position of the most intense peak of the layered zinc hydroxides, which are often found in corrosion products of zinc coatings. Under experimental conditions, and according to IR spectroscopy data, the layered zinc hydroxides can be either simonkolleite and/or hydrozincite. Table 2 shows the interplanar distances for the diffraction maximum at $2\theta \sim 11.5^\circ$ and the interlayer distances of various layered zinc hydroxides. In layered zinc hydroxides, this peak corresponds to the reflection from the layers containing zinc atoms in octahedral and tetrahedral coordination. Groups of atoms between the layers determine the interlayer distance and, accordingly, the position of the diffraction maximum.

The interplanar distance changed slightly with increasing exposure of the coatings to the corrosive environment. In this case, the value of the interplanar distance was in between the interlayer distances typical of simonkolleite and of the recently described zinc hydroxide dihydrate [34], that is, Cl^- and OH^- -containing compounds. There were no other diffraction peaks of the layered structures. This might be caused by layer disorder in the layered zinc hydroxide.

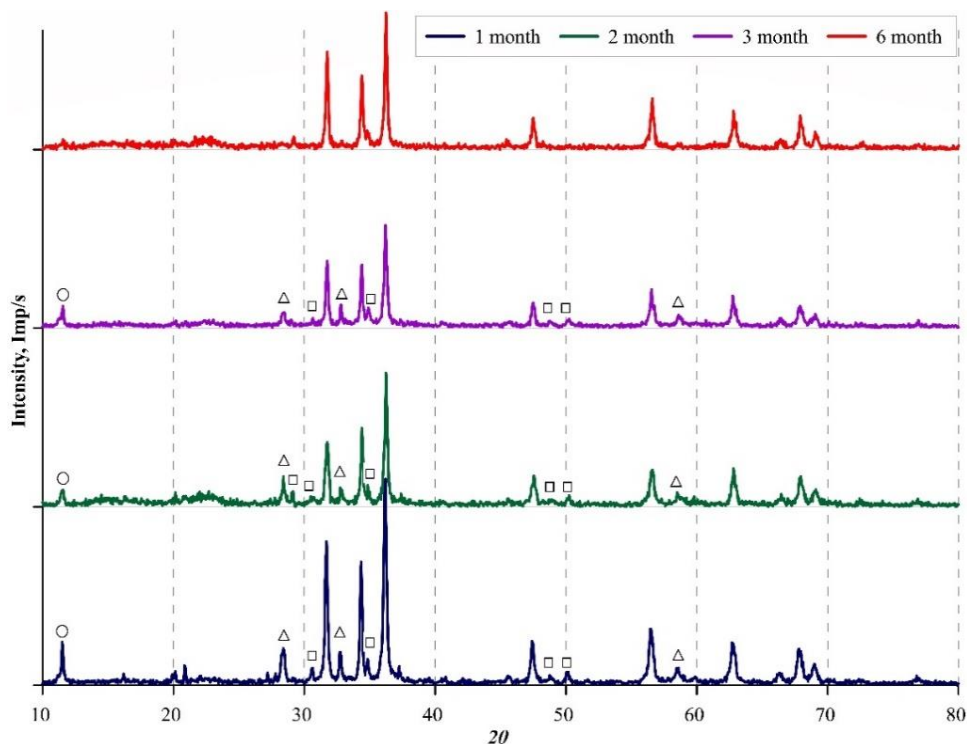


Figure 7. XRD spectra of the corrosion products formed on the DZ coatings after exposure in 3 wt.% NaCl of different duration (○ – layered zinc hydroxide; □ – ZnCl₂; Δ – NaCl; reflexes without name – ZnO).

Table 2. Interplanar distances corresponding to the peak 2θ ~ 11.5 on X-ray diffraction patterns of corrosion products at different exposures and interlayer distances for layered zinc hydroxides [34].

Time, months/compounds	<i>d</i> , Å
1	7.67
2	7.68
3	7.66
6	7.69
Simonkolleite Zn ₅ (OH) ₈ Cl ₂	7.88
Layered hydroxide Zn ₅ (OH) ₈ (OH) ₂ ·2H ₂ O	7.53
Hydrozincite Zn ₅ (OH) ₆ (CO ₃) ₂	6.86

In layered zinc hydroxides, this peak corresponds to reflection from layers containing zinc atoms in octahedral and tetrahedral coordination. Groups of atoms between layers determine the interlayer distance and, accordingly, the position of the diffraction maximum. The interplanar distance changes little with increasing exposure of coatings to a corrosive environment. In this case, the value of the interplanar distance is between the interlayer distances for simonkolleite and the recently described zinc hydroxide dihydrate [34], that is, Cl⁻ and OH⁻-containing compounds.

There are no other diffraction peaks of layered structures. This may be caused by disorder in the layers of layered zinc hydroxide.

3.3.4. Photoelectron spectroscopy of the corrosion products

Figure 8 shows XPS spectra taken from the surface of the coatings after exposure to a 3 wt.% NaCl for 1, 2, 3 and 6 months.

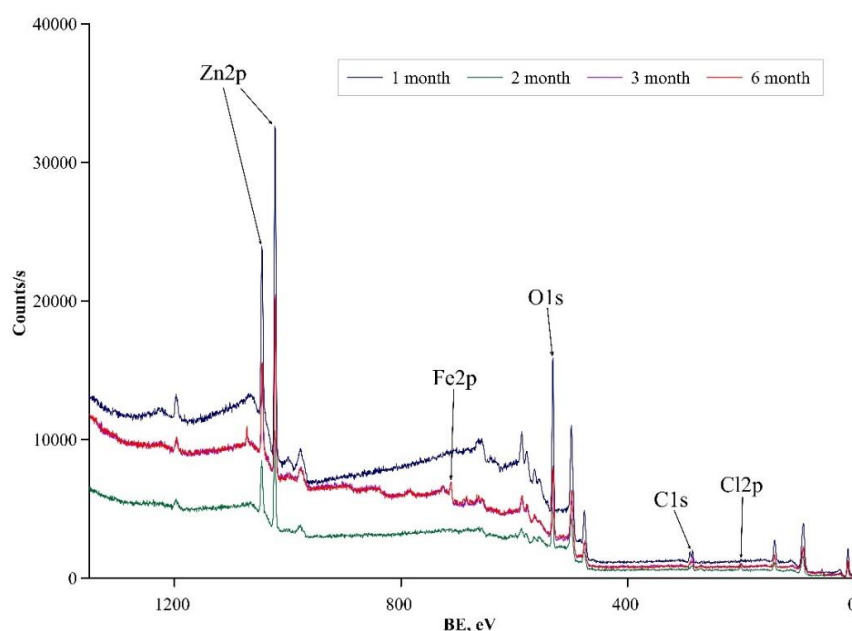


Figure 8. XPS spectra of the corrosion products formed on the DZ coatings after exposure in 3 wt.% NaCl of different duration.

Table 3 shows the elemental composition of the surface of the corrosion product layer. The concentration of chlorine on the surface of the layer of corrosion products increased after exposure for more than 2 months. Iron also appeared in the corrosion products only with increasing exposure for more than 2 months. The concentration of iron in the corrosion products increased significantly only after 3 months. Carbon concentration decreased with increasing exposure. The oxygen concentration is in the range from 40 to 50 at.%.

Table 3. Chemical composition of corrosion products layer according to XPS spectroscopy.

Time, months	1	2	3	6
Element	at.%			
C1s	18.03	16.26	14.40	12.34
Cl2p	0.59	2.78	2.10	2.10
Fe2p	–	2.44	8.53	7.71
O1s	47.67	41.04	49.45	43.56
Zn2p	33.71	37.48	25.53	32.30

Figure 9 shows the XPS spectra of the elements in details. Fe2p spectra after exposure for 2 months demonstrate a higher intensity of satellites, in comparison with the Fe2p spectra after exposure for 3 and 6 months. Differences in satellite intensity may indicate differences in corrosion products at different exposures. Iron is present as ferric chloride in the coating corrosion products after 2 months. Ferric chloride transforms into iron oxide or hydroxide after three months of exposure.

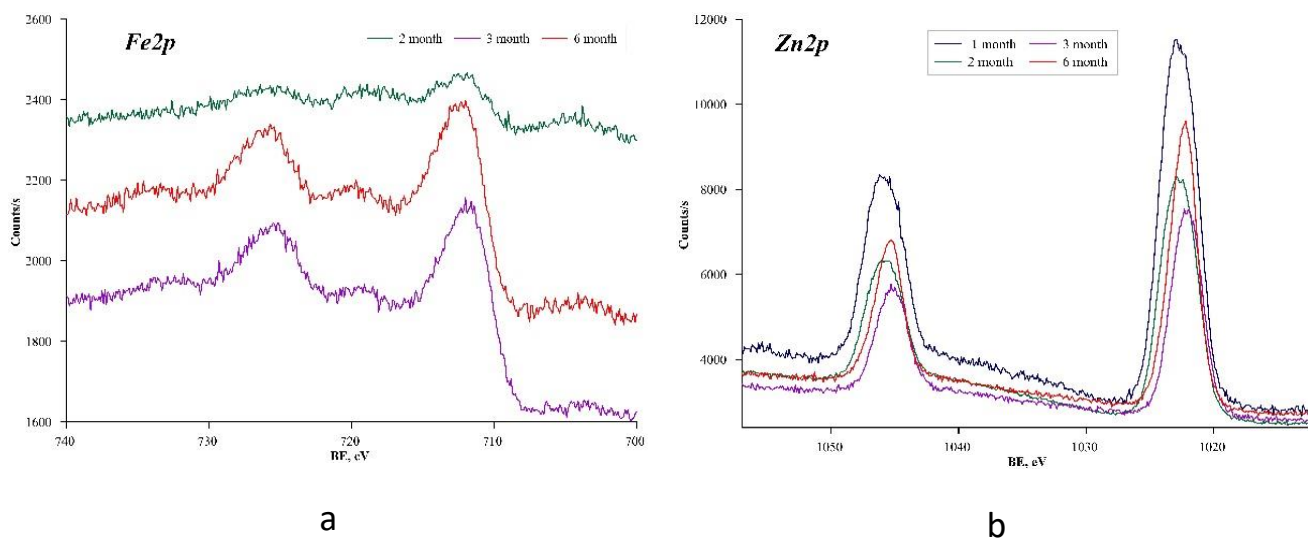
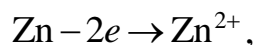


Figure 9. Fe2p (a) and Zn2p (b) XPS spectra of the corrosion products formed on the DZ coatings after exposure in 3 wt.% NaCl of different duration.

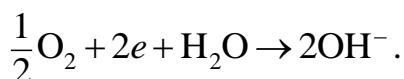
Zn2p spectra (Figure 9b) in the corrosion products after exposure for 1 and 2 months have larger linewidth compared to the spectra after 3 and 6 months of exposure. The spectra of the corrosion products after exposure for 1 and 2 months can be decomposed into two components with binding energies of 1021.7 eV and 1023.2 eV. The component with the binding energy of 1021.7 eV corresponds to zinc metal. The component with the binding energy of 1023.2 eV corresponds to zinc compounds of undetermined nature. At the same time, the spectra of zinc Zn2p corrosion products after exposure for 3 and 6 months have one component with a binding energy of about 1022.2 eV, which can be attributed to zinc oxide.

4. Discussion

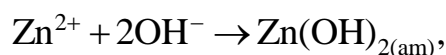
It is known that zinc corrosion is a set of Zn oxidation reactions at localized anodic sites:



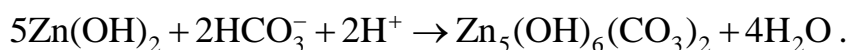
and O₂ reduction at the cathode sites:



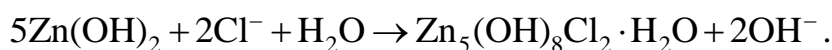
The main corrosion product is amorphous zinc hydroxide:



which can be transformed, depending on conditions, into zinc oxide ZnO or into crystalline β -Zn(OH)₂. When a corrosive environment contacts with air, carbon dioxide dissolves in the environment and turns into CO₃²⁻ and HCO₃⁻ ions, and hydrozincite can be formed by the reaction between Zn(OH)₂ and HCO₃⁻ [27, 28]:



At a relatively high concentration of chloride ions Zn(OH)₂ can be transformed into simonkolleite [29–32]:

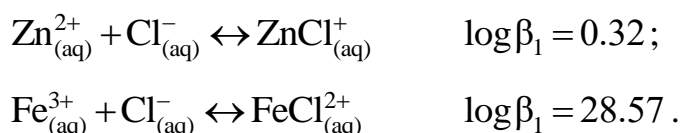


The authors of [35–37] reported that zinc corrosion products had protective properties due to simonkolleite. The rate of the coating corrosion decreases if the corrosion products layer is uniform, compact, non-porous with low electrical conductivity. It is important to take into account that corrosion can occur through the mechanism of selective dissolution of a more electronegative component if the coating is a zinc-based solid solution or an intermetallic compound. The matter is the surface roughness of the coating increases during this process, and this increase contributes to the formation of a more compact, uniform layer of corrosion products. Over time, selective dissolution can turn into co-dissolution of metals. Then the substances of other coating component appear in the layer of corrosion products, along with the zinc substances.

After 1 month of exposure of the zinc-based DZ coatings under study to 3 wt.% NaCl solution, iron is absent both in the corrosive environment and in the layer of corrosion products (Table 3). The ratio of Fe and Zn concentrations on the surface of coatings after corrosion is close to the ratio of metals in the coating before corrosion. Corrosion of the coatings with a thickness of 40±5 microns based on the δ -phase occurs through the mechanism of selective dissolution of zinc upon exposure for 1 month in a solution of 3 wt.% NaCl. The layer of corrosion products after 1 month exposure consists of ZnO and layered zinc hydroxide. There are no crystalline forms of simonkolleite or hydrozincite. Apparently, crystallization of amorphous Zn(OH)₂ into simonkolleite or hydrozincite is difficult under the conditions studied. However, chlorine and carbon are present in the layer of corrosion products according to XPS spectra. This can be explained by the sorption of a certain amount of Cl⁻ ions or CO₃²⁻ ions on layered zinc hydroxide. At the same time, basic zinc salts may be present in the layer of corrosion products in an amorphous state. In this state, they do not produce reflections in diffraction patterns, but corresponding absorption bands may appear in the IR spectra. The corrosion current does not decrease after exposure of the coating for 1 month (Table 1), despite the resistance of the layer of corrosion products. Apparently, the layer of products after 1 month exposure has rather weak protective properties.

After 2 months of exposure, iron is present in the corrosion products. The concentration of chlorine in the products increases by 5 times compared to that after 1 month exposure. Thus, the selective dissolution of zinc is replaced by simultaneous dissolution of Zn and Fe. IR and XPS spectra do not allow to unambiguously determine the chemical compound of iron in the corrosion products. However, based on the position of the satellites in the XPS spectra, it can be assumed that this is a ferric chloride or another complex compound with Cl^- ligands. The intensity of the absorption bands of simonkolleite increases in the IR spectra, but crystallization of simonkolleite is not observed, according to XRD. Thus, weakly bound Cl^- ions accumulate in the corrosion products and this can significantly accelerate the dissolution of iron.

If the solution contains Zn^{2+} , Fe^{3+} and Cl^- , then there may be equilibria between them:



Here β is the stability constant of the complex compound. The stability constant of FeCl^{2+} is by two orders of magnitude higher than that of ZnCl^+ . At the same time, the stability constant of FeOH^{2+} is by five orders of magnitude higher than that of ZnOH^+ [38]. Thus, the formation of chloride and hydroxo complexes of Fe^{3+} is thermodynamically more likely with the simultaneous dissolution of metals.

The corrosion rate of the coatings decreases as the exposure duration increases, whereas the resistance of ion transport through the corrosion product layer increases and has a maximum value after 2 months of exposure. Removing the layer of corrosion products increases i_{corr} . This suggests that the corrosion product layer effectively protects the coating from corrosion.

After exposure for 3 and 6 months, the concentration of chlorine in the corrosion product layer stabilizes, and the concentration of Fe increases by 3.5 times. The intensity of the absorption bands in the IR spectra, which relate to simonkolleite and hydrozincite, decreases. After 6 months of corrosion, only the absorption band of OH^- stretching vibrations has a high intensity in the IR spectra. The reflection of layered zinc hydroxide disappears from the diffraction patterns. Apparently, Fe^{3+} ions compete with Zn^{2+} for H_2O molecules, Cl^- and OH^- ions during long-term corrosion of DZ coatings. Iron inhibits the crystallization of basic zinc salts in the corrosion product layer. Also, Fe^{3+} ions are hydrolyzed in aqueous solutions, and the pH value near the electrode decreases. Because of this, zinc hydroxyl salts can be destroyed, since they are unstable in acidic environments.

This is consistent with the results obtained in [39–43], where Zn base salts were chemically precipitated in the presence of Fe ions. The authors showed that simonkolleite did not precipitate in the presence of Fe^{3+} ions in the electrolyte. A compact precipitate of small, poorly crystallized ZnO particles was formed instead of simonkolleite. At the same time, complex hydroxides $\text{Fe}(\text{OH})_x^{(3-x)+}$ were formed as a result of hydrolysis. They

condensed into amorphous iron oxides/hydroxides, and the compactness of the corrosion products of the layer increased [43].

Zinc oxide ZnO is the only crystalline corrosion product of the coatings after 6 months of corrosion. As a semiconductor, it reduces the electric resistance of the corrosion product layer, which should negatively affect the protection of the coating. However, the corrosion rate of DZ coatings stabilizes, and the corrosion current increases when the corrosion products layer is removed. This can be explained by the high density and compactness of the corrosion product layer that creates a barrier for oxygen and corrosive ions.

5. Conclusion

We studied the corrosion of 40 ± 5 μm thick DZ coatings based on the δ -phase FeZn_{7-10} in 3 wt.% NaCl solution under static conditions, full continuous immersion, without electrolyte renewal throughout the experiment. At the initial stage, corrosion of the coatings is accompanied by selective dissolution of zinc. This leads to the formation of zinc corrosion products, including basic layered hydroxides, which provide high corrosion resistance of the coatings. After 2 months of corrosion, the selective dissolution of zinc is replaced by the simultaneous dissolution of zinc and iron. The dissolution of iron is accompanied by a local change in the composition of the electrolyte due to hydrolysis, which leads to the destruction of layered zinc hydroxides with the formation of crystalline zinc oxide, which does not provide high corrosion resistance of coatings. However, even with a prolonged corrosion in chloride solutions, the basic compounds of zinc and iron in the amorphous state are spectroscopically determined in the corrosion products.

Reference

1. A.R. Marder, The metallurgy of zinc-coated steel, *Prog. Mater. Sci.*, 2000, **45**, no. 3, 191–275. doi: [10.1016/S0079-6425\(98\)00006-1](https://doi.org/10.1016/S0079-6425(98)00006-1)
2. E.V. Proskurkin and N.S. Gorbunov, Galvanizing Sherardizing and Other Zinc Diffusion Coatings, Technicopy Limited, Gloucestershire, 1972, 261 pp.
3. F. Natrup and W. Graf, 20 - Sherardizing: corrosion protection of steels by zinc diffusion coatings, *Thermochemical Surface Engineering of Steels*, 2015, 737–750. doi: [10.1533/9780857096524.5.737](https://doi.org/10.1533/9780857096524.5.737)
4. A.I. Biryukov, R.G. Galin, D.A. Zakharyevich, A.V. Wassilkowska and T.V. Batmanova, The effect of the chemical composition of intermetallic phases on the corrosion of thermal diffusion zinc coatings, *Surf. Coat. Technol.*, 2019, **372**, 166–172. doi: [10.1016/j.surfcoat.2019.05.029](https://doi.org/10.1016/j.surfcoat.2019.05.029)
5. A.I. Biryukov, R.G. Galin, D.A. Zakharyevich, A.V. Wassilkowska, A.V. Kolesnikov and T.V. Batmanova, A Layer-by-Layer Analysis of the Corrosion Properties of Diffusion Zinc Coatings, *Arch. Metall. Mater.*, 2020, **65**, no. 1, 99–102. doi: [10.24425/amm.2019.131101](https://doi.org/10.24425/amm.2019.131101)

6. A.I. Biryukov, R.G. Galin, D.A. Zakharyevich and A.P. Tronov, Formation and structure of simonkolleite on the surface of thermal diffusion zinc coatings in chloride-containing media, *Korrozi.: Mater., Zashch. (Corrosion: Materials, Protection)*, 2016, **9**, 28–33 (in Russian).
7. I.O. Wallinder and C. Leygraf, A critical review on corrosion and runoff from zinc and zinc-based alloys in atmospheric environments, *Corrosion*, 2017, **73**, no. 9, 1060–1077. doi: [10.5006/2458](https://doi.org/10.5006/2458)
8. R. Lindström, J.-E. Svensson and L.-G. Johansson, The atmospheric corrosion of zinc in the presence of NaCl the influence of carbon dioxide and temperature. *J. Electrochem. Soc.*, 2000; **147**, no. 5, 1751. doi: [10.1149/1.1393429](https://doi.org/10.1149/1.1393429)
9. T.H. Muster and I.S. Cole, The protective nature of passivation films on zinc: surface charge, *Corros. Sci.*, 2004, **46**, no. 9, 2319–2335. doi: [10.1016/j.corsci.2004.01.002](https://doi.org/10.1016/j.corsci.2004.01.002)
10. K. Morimoto, K. Tamura, S. Anraku, T. Sato, M. Suzuki and H. Yamada, Synthesis of Zn–Fe layered double hydroxides via an oxidation process and structural analysis of products, *J. Solid State Chem.*, 2015, **228**, 221–225. doi: [10.1016/j.jssc.2015.04.045](https://doi.org/10.1016/j.jssc.2015.04.045)
11. D. Persson, D. Thierry and O. Karlsson, Corrosion and corrosion products of hot dipped galvanized steel during long term atmospheric exposure at different sites world-wide, *Corros. Sci.*, 2017, **126**, 152–165. doi: [10.1016/j.corsci.2017.06.025](https://doi.org/10.1016/j.corsci.2017.06.025)
12. D. Thierry and N. LeBozec, Corrosion products formed on confined hot-dip galvanized steel in accelerated cyclic corrosion tests, *Corrosion*, 2009, **65**, no. 11, 718–725. doi: [10.5006/1.3319098](https://doi.org/10.5006/1.3319098)
13. O.A. Kozaderov, O.V. Koroleva and A.V. Vvedenskii, Kinetics of phase transformations in a binary alloy surface layer at the selective dissolution. I. Theoretical analysis, *Prot. Met. Phys. Chem. Surf.*, 2009, **45**, 31–35. doi: [10.1134/S2070205109010043](https://doi.org/10.1134/S2070205109010043)
14. A.V. Vvedenskii, S. Grushevskaya, D. Kudryashov and S. Ganzha, The influence of the conditions of the anodic formation and the thickness of Ag (I) oxide nanofilm on its semiconductor properties, *J. Solid State Electrochem.*, 2010, **14**, 1401–1413. doi: [10.1007/s10008-009-0952-9](https://doi.org/10.1007/s10008-009-0952-9)
15. O.A. Kozaderov and A.V. Vvedenskii, Voltamperometry of selective dissolution of Ag–Au alloys under conditions of solid phase-liquid phase mass transfer, *Prot. Met. Phys. Chem. Surf.*, 2013, **49**, 724–733. doi: [10.1134/S2070205113060099](https://doi.org/10.1134/S2070205113060099)
16. P. Volovitch, T.N. Vu, C. Allely, A.A. Aal and K. Ogle, Understanding corrosion via corrosion product characterization: II. Role of alloying elements in improving the corrosion resistance of Zn–Al–Mg coatings on steel, *Corros. Sci.*, 2011, **53**, no. 8, 2437–2445. doi: [10.1016/j.corsci.2011.03.016](https://doi.org/10.1016/j.corsci.2011.03.016)
17. A.I. Biryukov, O.A. Kozaderov, R.G. Galin, D.A. Zakharyevich and V.E. Zhivulin, Details of the mechanism of dissolution of iron-zinc coatings based on the δ -phase in acidic media, *Int. J. Corros. Scale Inhib.*, 2020, **9**, no. 4, 1477–1489. doi: [10.17675/2305-6894-2020-9-4-18](https://doi.org/10.17675/2305-6894-2020-9-4-18)

18. A.I. Biryukov, O.A. Kozaderov, D.A. Zakharyevich, R.G. Galin, L.O. Burmistrov, T.V. Batmanova and V.E. Zhivulin, Corrosion of diffusion iron–zinc coatings (δ -phase) in an alkaline medium, *Int. J. Corros. Scale Inhib.*, 2021, **10**, no. 4, 1677–1688. doi: [10.17675/2305-6894-2021-10-4-19](https://doi.org/10.17675/2305-6894-2021-10-4-19)
19. RF Patent 2170643, C23C10/28, B22F1/02, R.G. Galin, *Modified zinc powder*, 2001 (in Russian).
20. R.G. Galin, D.A. Zakharyevich and S.V. Rushchits, Formation and structure of diffusional zinc coatings formed in nanocrystallized zinc powders, *Mater. Sci. Forum*, 2016, **870**, 404–408. doi: [10.4028/www.scientific.net/MSF.870.404](https://doi.org/10.4028/www.scientific.net/MSF.870.404)
21. A.I. Biryukov, D.A. Zakharyevich, T.V. Batmanova, R.G. Galin, M.N. Ulyanov and V.E. Zhivulin, Corrosion of diffusion zinc coatings in sodium chloride solutions, *Chim. Techno Acta*, 2022, **9**, no. 4, 20229421. doi: [10.15826/chimtech.2022.9.4.21](https://doi.org/10.15826/chimtech.2022.9.4.21)
22. D. Persson, D. Thierry and N. LeBozec, Corrosion product formation on Zn55Al coated steel upon exposure in a marine atmosphere, *Corros. Sci.*, 2011, **53**, no. 2, 720–726. doi: [10.1016/j.corsci.2010.11.004](https://doi.org/10.1016/j.corsci.2010.11.004)
23. R. Autengruber, G. Luckeneder and A.W. Hassel, Corrosion of press-hardened galvanized steel, *Corros. Sci.*, 2012, **63**, 12–19. doi: [10.1016/j.corsci.2012.04.048](https://doi.org/10.1016/j.corsci.2012.04.048)
24. O.K. Srivastava and E.A. Secco, Studies on metal hydroxy compounds. II. Infrared spectra of zinc derivatives ϵ -Zn(OH)₂, β -ZnOHCl, ZnOHF, Zn₅(OH)₈Cl₂ and Zn₅(OH)₈Cl₂·H₂O, *Can. J. Chem.*, 1967, **45**, no. 6, 585–588. doi: [10.1139/v67-097](https://doi.org/10.1139/v67-097)
25. T.N. Vu, P. Volovitch and K. Ogle, The effect of pH on the selective dissolution of Zn and Al from Zn–Al coatings on steel, *Corros. Sci.*, 2013, **67**, 42–49. doi: [10.1016/j.corsci.2012.09.042](https://doi.org/10.1016/j.corsci.2012.09.042)
26. M. Keddam, A. Hugot-Le-Goff, H. Takenouti, D. Thierry and M.C. Arevalo, The influence of a thin electrolyte layer on the corrosion process of zinc in chloride-containing solutions, *Corros. Sci.*, 1992, **33**, no. 8, 1243–1252. doi: [10.1016/0010-938X\(92\)90133-N](https://doi.org/10.1016/0010-938X(92)90133-N)
27. F. Zhu, D. Persson, D. Thierry and C. Taxen, Formation of corrosion products on open and confined zinc surfaces exposed to periodic wet/dry conditions, *Corrosion*, 2000, **56**, no. 12, 1256–1265. doi: [10.5006/1.3280514](https://doi.org/10.5006/1.3280514)
28. Q. Qu, L. Li, W. Bai, C. Yan and C. Cao, Effects of NaCl and NH₄Cl on the initial atmospheric corrosion of zinc, *Corros. Sci.*, 2005, **47**, no. 11, 2832–2840. doi: [10.1016/j.corsci.2004.11.010](https://doi.org/10.1016/j.corsci.2004.11.010)
29. T.H. Muster and I.S. Cole, The protective nature of passivation films on zinc: surface charge, *Corros. Sci.*, 2004, **46**, no. 9, 2319–2335. doi: [10.1016/j.corsci.2004.01.002](https://doi.org/10.1016/j.corsci.2004.01.002)
30. K. Morimoto, K. Tamura, S. Anraku, T. Sato, M. Suzuki and H. Yamada, Synthesis of Zn–Fe layered double hydroxides via an oxidation process and structural analysis of products, *J. Solid State Chem.*, 2015, **228**, 221–225. doi: [10.1016/j.jssc.2015.04.045](https://doi.org/10.1016/j.jssc.2015.04.045)
31. D. Persson, D. Thierry and O. Karlsson, Corrosion and corrosion products of hot dipped galvanized steel during long term atmospheric exposure at different sites world-wide, *Corros. Sci.*, 2017, **126**, 152–165. doi: [10.1016/j.corsci.2017.06.025](https://doi.org/10.1016/j.corsci.2017.06.025)

32. D. Thierry and N. LeBozec, Corrosion products formed on confined hot-dip galvanized steel in accelerated cyclic corrosion tests, *Corrosion*, 2009, **65**, no. 122, 718–725. doi: [10.5006/1.3319098](https://doi.org/10.5006/1.3319098)
33. Q. Qu, C. Yan, Y. Wan and C. Cao, Effects of NaCl and SO₂ on the initial atmospheric corrosion of zinc, *Corros. Sci.*, 2002, **44**, no. 12, 2789–2803. doi: [10.1016/S0010-938X\(02\)00076-8](https://doi.org/10.1016/S0010-938X(02)00076-8)
34. A. Gordeeva, Y.-J. Hsu, I.Z. Jenei, P.H.B. Brant Carvalho, S.I. Simak, O. Andersson and U. Haussermann, Layered Zinc Hydroxide Dihydrate, Zn₅(OH)₁₀·2H₂O, from Hydrothermal Conversion of ε-Zn(OH)₂ at Gigapascal Pressures and its Transformation to Nanocrystalline ZnO, *ACS Omega*, 2020, **5**, no. 28, 17617–17627. doi: [10.1021/acsomega.0c02075](https://doi.org/10.1021/acsomega.0c02075)
35. J.D. Yoo, P. Volovitch, A.A. Aal, C. Allely and K. Ogle, The effect of an artificially synthesized simonkolleite layer on the corrosion of electrogalvanized steel, *Corros. Sci.*, 2013, **70**, 1–10. doi: [10.1016/j.corsci.2012.10.024](https://doi.org/10.1016/j.corsci.2012.10.024)
36. J.D. Yoo, K. Ogle and P. Volovitch, The effect of synthetic zinc corrosion products on corrosion of electrogalvanized steel: I. Cathodic reactivity under zinc corrosion products, *Corros. Sci.*, 2014, **81**, 11–20. doi: [10.1016/j.corsci.2013.11.045](https://doi.org/10.1016/j.corsci.2013.11.045)
37. J.D. Yoo, K. Ogle and P. Volovitch, The effect of synthetic zinc corrosion products on corrosion of electrogalvanized steel. II. Zinc reactivity and galvanic coupling zinc/steel in presence of zinc corrosion products, *Corros. Sci.*, 2014, **83**, 32–37. doi: [10.1016/j.corsci.2013.12.024](https://doi.org/10.1016/j.corsci.2013.12.024)
38. Y.Y. Lurie, *Handbook of Analytical Chemistry*, Khimiya, Moscow, 1971, 454 pp. (in Russian).
39. T. Ishikawa, K. Matsumoto, A. Yasukawa, K. Kandori, T. Nakayama and T. Tsubota, Influence of metal ions on the formation of artificial zinc rusts, *Corros. Sci.*, 2004, **46**, no. 2, 329–342. doi: [10.1016/S0010-938X\(03\)00155-0](https://doi.org/10.1016/S0010-938X(03)00155-0)
40. T. Ishikawa, M. Murai, K. Kandori and T. Nakayama, Structure and composition of artificially synthesized rusts of Zn–Fe and Zn–Ti alloys, *Corros. Sci.*, 2006, **48**, no. 10, 3172–3185. doi: [10.1016/j.corsci.2005.11.015](https://doi.org/10.1016/j.corsci.2005.11.015)
41. H. Tanaka, A. Fujioka, A. Futoyu, K. Kandori and T. Ishikawa, Synthesis and characterization of layered zinc hydroxychlorides, *J. Solid State Chem.*, 2007, **180**, no. 7, 2061–2066. doi: [10.1016/j.jssc.2007.05.001](https://doi.org/10.1016/j.jssc.2007.05.001)
42. K. Morimoto, K. Tamura, S. Anraku, T. Sato, M. Suzuki and H. Yamada, Synthesis of Zn–Fe layered double hydroxides via an oxidation process and structural analysis of products, *J. Solid State Chem.*, 2015, **228**, 221–225. doi: [10.1016/j.jssc.2015.04.045](https://doi.org/10.1016/j.jssc.2015.04.045)
43. H. Tanaka, J. Wakatsuki, K. Kandori, T. Ishikawa and T. Nakayama, Role of zinc compounds on the formation, morphology, and adsorption characteristics of β-FeOOH rusts, *Corros. Sci.*, 2010, **52**, no. 9, 2973–2978. doi: [10.1016/j.corsci.2010.05.010](https://doi.org/10.1016/j.corsci.2010.05.010)

